

Hybrid Arc/Glow Microdischarges at Atmospheric Pressure and Their Use in Portable Systems for Liquid and Gas Sensing

Bhaskar Mitra, Brandon Levey, and Yogesh B. Gianchandani

Abstract—This paper reports on dc pulse-powered microdischarges in air at atmospheric pressure and their potential utility in chemical sensing. For electrode gaps of 50–100 μm , microdischarges take the form of a glow discharge, an arc discharge, or a hybrid of the two. Arc microdischarges have high optical intensity but suffer from high background emission. Glow microdischarges have low background emission, but the prominent emission is confined in the UV–blue region of the spectrum. The arc–glow hybrid has characteristics that are intermediate between the two and can be tuned by circuitry to suit the chemical sensing application. A handheld system for chemical analysis using synchronized emission spectroscopy of these pulsed microdischarges is demonstrated. The system employs an exchangeable sensor chip (different for gas and liquid samples), a control circuit, and a commercially available portable spectrum analyzer coupled to a handheld computer. A pump and inert carrier gases are not utilized. The system can generate one or a series of single-shot microdischarges per chemical analysis. The gas discharge microchip, which utilizes electroplated copper electrodes on a glass substrate, has an electrode separation of 75 μm and an active area of $300 \times 300 \mu\text{m}^2$. The handheld system has been used to detect 17 ppm of acetone vapor in air. The liquid discharge microchip also has an electrode gap of 75 μm and an active area of $1 \times 1 \text{ mm}^2$. It uses a porous cathode fabricated by micromolding and sintering glass frit slurry in a microchannel. When a microdischarge is initiated between the metal anode and the wet cathode, the liquid is sputtered into the microdischarge and emits characteristic line spectra. In this configuration, the system can detect 2 ppm of aqueous Cr without preconcentration.

Index Terms—Chemical sensing systems, gas detectors, gas discharge devices, microarc, microdischarge, microplasma, water chemistry.

I. INTRODUCTION

TO MEET the challenges posed by globalization and environmental pollution, there is an increasing need for point-of-use chemical analysis. Conventional devices like chromatographs and mass spectrometers must be complemented by fast, efficient, flexible, and portable devices. Emission spectroscopy of pulsed microdischarges at atmospheric pressure is

Manuscript received January 26, 2008; revised April 13, 2008. This work was supported in part by the National Science Foundation.

B. Mitra and Y. B. Gianchandani are with the Department of Electrical Engineering and Computer Science, University of Michigan, Ann Arbor, MI 48109 USA (e-mail: bmitra@umich.edu; yogesh@umich.edu).

B. Levey was with the Department of Electrical Engineering and Computer Science, University of Michigan, Ann Arbor, MI 48109 USA. He is now with Sandia National Laboratories, Albuquerque, NM 87185-1194 USA.

Color versions of one or more of the figures in this paper are available online at <http://ieeexplore.ieee.org>.

Digital Object Identifier 10.1109/TPS.2008.927135

appealing for highly portable sensing of gas and vapor because it reduces the need for pumps. Powering the discharge with pulsed dc can also eliminate the need for bulky RF power sources, thereby reducing system complexity and improving form factor. By using electrical discharges between microelectrodes, it is possible to realize glow microdischarges at atmospheric pressure. In this paper, we show that the resulting discharge shows properties intermediate between arc and glow discharges.

Existing options for miniaturized microsensors, including surface-acoustic-wave devices, chemiresistors, chemicapacitors, chemimechanical sensors, and metal oxide sensors which measure change in properties of thin films, have been demonstrated for sensing of toxic vapors [1]. Ion-selective field-effect transistors and amperometric and potentiometric sensors, which measure changes in electrochemical properties of a solution, have been developed for chemical sensing in aqueous environments [2]. However, despite some excellent progress over the years, their use remains limited to specific chemicals in controlled environments. This is at least in part due to challenges in controlling thin-film properties and the difficulty in making stable miniature reference electrodes.

Virtually all these sensors have cross-sensitivities to many different chemicals, and false positives pose an additional challenge. One way to address this is to employ an array of different sensors instead of a single sensor. Even though each sensor is not adequately specific, the overall signature is highly specific [3]. Arrayed sensors are also useful for analyzing simple mixtures of gases. However, more complex mixtures additionally require the use of a gas chromatography system, which first separates the mixtures based on elution time of the constituents. These have been very successful in the separation of complex mixtures, even those containing very low concentrations of organic vapors. Because gas chromatographs do not provide complete separation or chemical identification, a sensor is needed for accurate chemical recognition and elimination of false positives. Furthermore, systems using gas chromatographs are restricted to mostly organic vapors and leave a wide range of inorganic gases outside their scope.

There has been considerable effort directed toward micro-machined mass spectrometry systems, but progress has been hampered because many of the phenomena do not scale favorably [6]. They also require very high vacuum, which is difficult to achieve using microscale pumps. Miniature spectrometers based on quadruple mass filters [7] and differential ion mobility

[8] that can operate at atmospheric pressure have recently been reported. Of these, the latter has shown significant promise and can resolve even isomers. However, it is a separation technique for ions rather than an identification technique, and each species needs to be calibrated for the applied field conditions. It is also very sensitive to humidity in air, and hence, the sensor has to be used in a controlled ambient.

Microdischarge-based spectral sensors, like mass spectrometers, detect chemicals based on their atomic structure rather than their chemical properties. Discharge spectroscopy in the form of inductively coupled plasma atomic emission spectroscopy is one of the most sensitive techniques used in laboratories by chemists [9] and is commonly used with gas chromatography systems. Many groups (including ours) have miniaturized microplasmas to chip scale for chemical sensing and other applications [10]. A variety of powering schemes have been reported for these discharges; a detailed review is presented in [11]. Broekaert [12] developed RF microplasmas for chemical sensing using diode laser atomic absorption spectroscopy. Hopwood developed inductively coupled microplasmas [13] and microwave plasmas operating at atmospheric pressures [14]. Park *et al.* [15] developed micro hollow cathode discharges for display and IR sensing applications. DC glow microdischarges for gas chromatography were reported by Eijkel *et al.* [16]. DC or pulsed discharges are appealing for use in handheld systems because they require simple circuitry and can be operated at atmospheric pressure.

One of the very attractive features of chemical sensing by emission spectroscopy is that it works for gas- [10] and liquid-phase [17] species. In the previous work, we have demonstrated low-power microdischarge gas/vapor sensors [18] and liquid electrode devices for the detection of trace elements in water samples [19], [20].

DC glow microdischarges that were previously explored for *in situ* deposition and etching applications [21] had a discharge gap of few hundred micrometers and were operated at reduced pressures (< 30 torr). For these discharges, the preferred breakdown path was a strong function of pressure and power levels. These discharges were surface discharges, and the glow was concentrated directly above the cathode, not in the interelectrode space as in conventional (and capillary) discharges. These discharges were also cold discharges, with mean electron temperatures on the order of 10 000 K. The electrons had a bimodal (nonequilibrium) distribution with a Maxwellian component for thermal electrons, and a high-energy tail corresponding to beam electrons. Such discharges are typically not in thermal equilibrium because the capture cross section for an inelastic collision between a high-energy electron and a low-energy neutral or ion is small (in an elastic collision, very little energy is transferred because of the low mass of the electron compared to the gas species). This results in lower gas temperatures and low plasma density. The discharge glow was concentrated in the UV–blue region of the spectrum. However, these discharges were unstable at pressures close to 1 atm and degenerated into arcs. Unlike glow microdischarges, which are driven by steady currents, arc microdischarges have high transient current. These typically result in optical emission over a wide spectral range covering both UV and infrared portions of the spectrum.

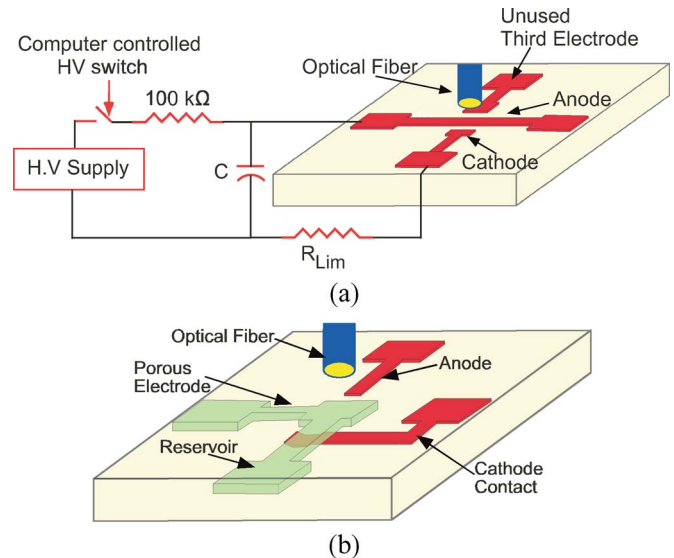


Fig. 1. (a) Schematic of the gas microdischarge chip. (b) The liquid microdischarge chip.

In this paper, we investigate arc–glow discharge hybrids at atmospheric pressure with coplanar microelectrode arrangements. We investigate the electrical and optical characteristics of these discharges and their dependence on circuit elements. We demonstrate that the discharge can be controllably varied by external circuit elements to provide spectral characteristics favorable for chemical sensing. These ideas are brought together, in the context of a handheld system, for the analysis of chemicals using microdischarges.¹ The system employs disposable gas and liquid discharge microchips (GDMs and LDMs, respectively) with a common interface. The LDM uses the same basic principle of using a liquid cathode, as described in [19] and [20], but using a porous cathode, instead of a microfluidic channel for sample delivery. This design permits controlled uptake of small volumes of the liquid sample and can be used to detect very low concentrations of metallic impurities in water samples. Both chips use atmospheric-pressure pulsed microdischarges and avoid the use of a preconcentrator to eliminate pumping demands.

All discharges investigated in this paper are pulsed discharges. This is done to reduce power consumption and increase device lifetime. Section II describes arc–glow discharge hybrids as well as the microfabricated devices. Section III describes the system design, and Section IV describes the measurement results.

II. ARC/GLOW BEHAVIOR AND DISCHARGE CHIPS

As noted previously, pulsed microdischarges at atmospheric pressure can exist as glow discharges, arc discharges, or intermediate hybrids. The control circuit used in this effort is shown in Fig. 1(a). The microdischarge is created by discharging a capacitor that has been previously charged to a high voltage (450–900 V). The reported measurements are performed with devices with electrode spacing of 75 μm ; the observations are

¹Portions of this work have been presented in conference abstract form in [23] and [24].

valid for devices with smaller and larger spacing and have been observed for devices spaced 50–100 μm apart. When the switch is turned on, the capacitor starts charging, and as soon as it reaches breakdown voltage, it discharges. A computer-controlled switch is used to control the time for which the discharge is on. A current-limiting resistor is used in the ground return path to regulate the discharge. The form of the discharge depends strongly on the limiting resistor.

A. Arc/Glow Behavior

When a large current-limiting resistor is used, the discharge takes a form similar to a glow. These kinds of discharges are referred to as “cold discharges” and are characterized by high-energy (temperature) electrons and low-energy (temperature) neutrals (gas molecules) existing in thermal nonequilibrium [25]. For microscale geometries, the glow is confined to a space over the cathode surface. Most of the applied voltage drops across a small space charge region close to the cathode, resulting in a localized region with high electric field.

Electrons are emitted from the cathode surface with low energies (< 1 eV) [26]. This is not sufficient for ionization of the gas medium, so the space next to the cathode is dark. The electrons gain energy as they are accelerated by the electric field between the electrodes, and as the electron energy rises to levels that are large enough to excite atoms, a *cathode glow region* appears. When the electron energy rises to a level such that the collision cross section for the excitation falls off, the electrons cease to excite atoms, and a *cathode dark space* is formed. This is the region where ionization (and avalanche multiplication) takes place and positive space charge builds up. The field near the cathode (from the cathode to the end of the cathode dark space) is extremely high and is the main driving force behind the glow discharge. At the end of the cathode layer, the electron flux gets fairly large, and electrons generated at the end of the region have moderate energies. This leads to the formation of an intense *negative glow* region. For small interelectrode gaps, and atmospheric pressure conditions, the negative glow and cathode glow overlap (these regions have finite thickness due to the spread in electron energy), and only one glow region is seen. In planar discharges, the optical characterization typically involves observations from above, so the spatial variation in the glow is not observed, and the glows appear as one.

In addition to the “bulk” electrons, which participate in the breakdown process, there are also many “beam” electrons [21], [22]. These electrons, which do not undergo many collisions, have extremely high energy. “Beam” electrons are formed because the capture cross section of collisions between electrons and ions or neutrals is a function of the electron energy. For high-energy electrons, this cross section is low because the interaction time between the electrons and the atom or molecule is small. Thus, some of the electrons, which do not undergo collisions in low-energy state, are accelerated to very high energy. These beam electrons, thus, do not contribute to the breakdown process and make the discharge less power efficient.

For a discharge to be self-sustaining, it needs a constant supply of electrons from the electrodes. In the case of glow microdischarges, these are supplied by secondary emission

from the cathode surface. Secondary emission occurs when positively charged ions, accelerated through the space charge region, hit the cathode surface and release electrons. Secondary emission is favored in conditions where the collision frequency of the ions is low, like in low-pressure discharges. Photoemission is another important source for initial electrons. In this process, the UV photons from the discharge cause electrons to be emitted from the cathode surface by photoelectric emission. Electrode processes thus play an important role in these dc and pulsed microdischarges, and the discharge is very sensitive to changes in the work function and surface quality of the electrode material. For example, under conditions that are otherwise identical, changing the electrode material can change the discharge from a glow to an arc. The third source of electrons in microdischarges is thermionic emission (or field-assisted thermionic emission). In glow microdischarges, the main source of electrode heating is positive-ion bombardment of the cathode. This heating causes a temporal variation in discharge characteristics in-between pulses and makes pulsed discharges very different from dc discharges.

The second mode of breakdown is the arc discharge. In an arc, the electric field is not as high as cold cathode discharges. Arcs can be of vapor arcs or thermionic arcs, which themselves can be of several kinds [28]. The arcs encountered in this paper are thermionic spot mode arcs at high pressure, as defined in [28]. The main source of electrons in an arc is thermionic emission from the cathode. Thermionic emission is a much more efficient process compared with secondary emission and photoemission, so only a few generations of avalanche multiplication are enough for the discharge to be self-sustaining. This is why arc discharges can be sustained at low voltages. For two terminal devices, arcs usually start as a glow discharge that then changes into an arc. Thus, the initiation voltage for a two-terminal arc is high, but the sustain voltage is low. The current, however, is high compared to glow discharge, because it must heat the electrode for thermionic emission. The emission usually starts from a local hot spot on the cathode surface, causing the arc microdischarge to appear as a narrow filament. Arc discharges exist in thermal equilibrium and have high plasma density. Because of this, the spectral distribution of an arc is very wide and spans the range from UV to infrared wavelengths. Arc microdischarges require much less current compared with conventional arc discharges. This is because arcs are driven primarily by thermionic emission, and it is easier to heat microelectrodes to high temperatures using less current. The volume of the air that is ionized in an arc microdischarge is also much lower as a result of scaling, which makes it easier to generate arc discharges with small interelectrode gaps. They are usually generated by discharging a small capacitor across an air gap. The small air gap enables the use of smaller capacitors (or smaller amounts of charge), which allows good control of the properties of the discharges by using a limiting resistor. Control of the properties of the discharge is important, as uncontrolled discharges can lead to rapid deterioration of the electrode surfaces.

In hybrid microdischarges, both arc and glow discharges are present together. Two different electrode processes take place simultaneously: (a) secondary emission from the cathode

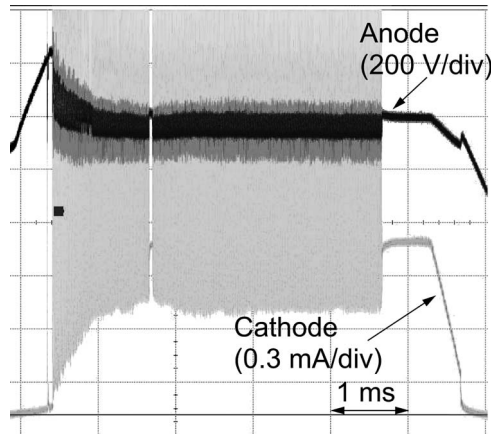


Fig. 2. Typical discharge voltage and current waveforms for an arc-glow hybrid discharge. The circuit configuration is as shown in Fig. 1(a). (Lower) The current waveform shows a steady component corresponding to the glow component, and current spikes (of 5–50- μ s duration, depending upon the values of circuit elements) corresponding to an arclike component of the discharge. The current spikes are accompanied by a drop in breakdown voltage, which is seen as an oscillation in the (upper) anode voltage waveform.

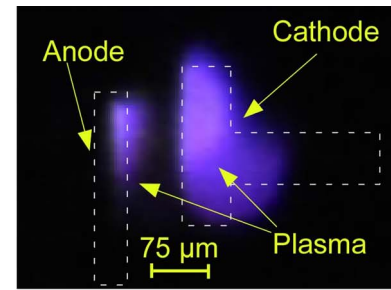
surface, which drives glowlike discharges; (b) thermionic emission from local cathode hotspots at which arclike discharges nucleate. In a conventional discharge, the glow discharge rapidly degenerates into an arc discharge, and the intermediate phase where both are present is very short and only appears as a transient phase [27]. In a microdischarge, however, owing to the dynamics of the discharge process and the small amount of charge delivered to the discharge, it is possible to realize such a stable intermediate.

To evaluate the electrical characteristics of the gas discharge microchip, an oscilloscope was used to examine the cathode and anode (through a 10-M Ω : 100-k Ω divider) waveforms. The anode waveform indicates the breakdown voltage, and the cathode waveform indicates the discharge current (drop across the limiting resistor). The discharge capacitor was 10 pF, and the limiting resistor was varied from 1 k Ω to 1 M Ω .

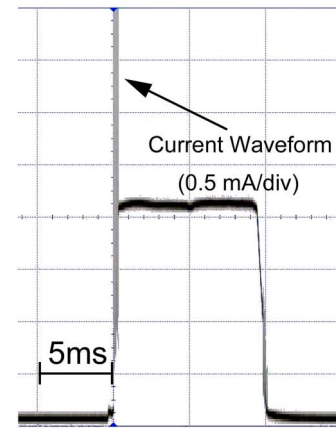
Fig. 2 shows the current and voltage waveforms of a typical atmospheric microdischarge for an applied voltage of 630 V. An overvoltage is applied for repeatability, and other reasons are outlined in Section IV. The initial breakdown occurs at a voltage of 630 V, but subsequently, the breakdown voltage decreases to 400 V. The current waveform is comprised of two parts—a steady component, and a transient component, which rides on the steady component. The steady component corresponds to a glowlike discharge present over the cathode, whereas the transient component corresponds to an arclike discharge present in between the electrodes. An oscillation corresponding to the arclike component is seen in the voltage waveform as well. The current in this state is approximately given by [27]

$$nev_d \exp \left(\int_0^d \alpha dx \right) + C \frac{dV}{dt} = \frac{V_0 - V}{Z} \quad (1)$$

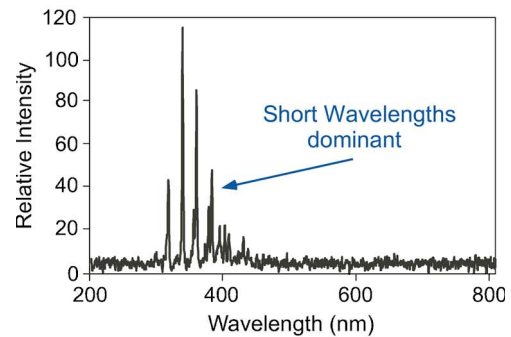
where n is the electron density, v_d is the drift velocity, α is the Townsend ionization coefficient, Z is the effective impedance, and $V_0 - V$ is the voltage drop across the series impedance. The arc current corresponds to the discharging of the capacitor (C),



(a)



(b)



(c)

Fig. 3. (a) Example of a glowlike discharge. The glow is confined to the cathode and near the anode. (b) Oscilloscope waveforms show a steady current. (c) Emission spectrum of the glowlike discharge in air.

whereas the glow discharge component represents the term on the left.

Fig. 3(a) shows a photograph of a glow microdischarge at atmosphere. The images of the transient discharge are captured by a video camera at 25 frames per second. A bright glow is seen in the region above the cathode and near the anode, with dark space in between. The discharge is characterized by a steady current throughout the duration of the discharge. Fig. 3(b) shows the current waveforms for such a glow discharge, measured by the voltage drop across the 100-k Ω current-limiting resistor to ground. A current spike is seen at the beginning of the discharge. Spectral characterization is performed by observing the discharge with a handheld Ocean Optics spectrometer. Fig. 3(c) shows the spectra for the glowlike discharge described earlier. The discharge shows a strong emission in the UV-blue region but very little emission in other

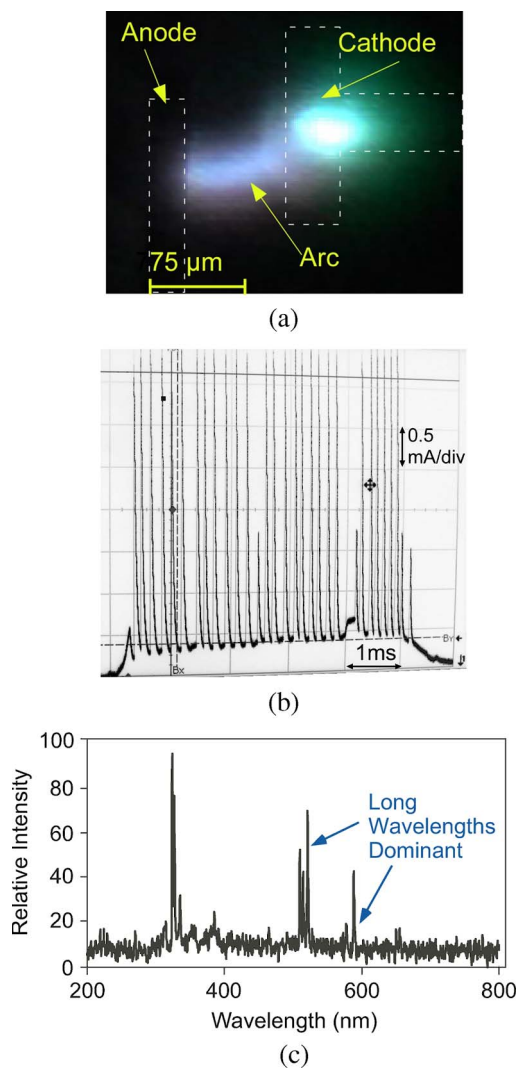


Fig. 4. (a) Example of an arclike discharge. (b) The current waveform shows that the discharge is powered by transient bursts of current. (c) Emission spectrum of an “arclike” discharge, with strong lines being in the (green) visible region of the spectrum but with weaker lines being in the UV–blue region. The spectrum is dominated by emission from copper (324.7, 327.33, 510.84, 515.8, and 522.07 nm).

regions of the spectrum. The blue color is primarily due to emission from N_2 second positive ($C^3\Pi - B^3\Pi$ —337.1, 357.5, 375.1, and 380.4 nm) and N_2^+ first negative ($B^2\Sigma_u^+ - X^2\Sigma_g^+$ —391.4 nm) systems.

When a small limiting resistor is used, the discharge is arclike. This allows for large transient currents necessary for rapid heating of the plasma. Fig. 4(a) shows the photograph of the discharge glow for an arclike microdischarge. The bright glow is present in the gap between the electrodes rather than over the electrodes and is much brighter compared to a glow discharge. The green emission at the cathode is copper emission from the cathode hot spot that powers the discharge. Fig. 4(b) shows the current waveform when using a 2.2-k Ω current-limiting resistor. The average current is 4.2 mA. The discharge is a succession of tiny discharges powered by high-current spikes. The capacitor repeatedly charges up to the breakdown voltage required for plasma formation and dumps all the charge stored in surges of current. There is a steady glowlike component,

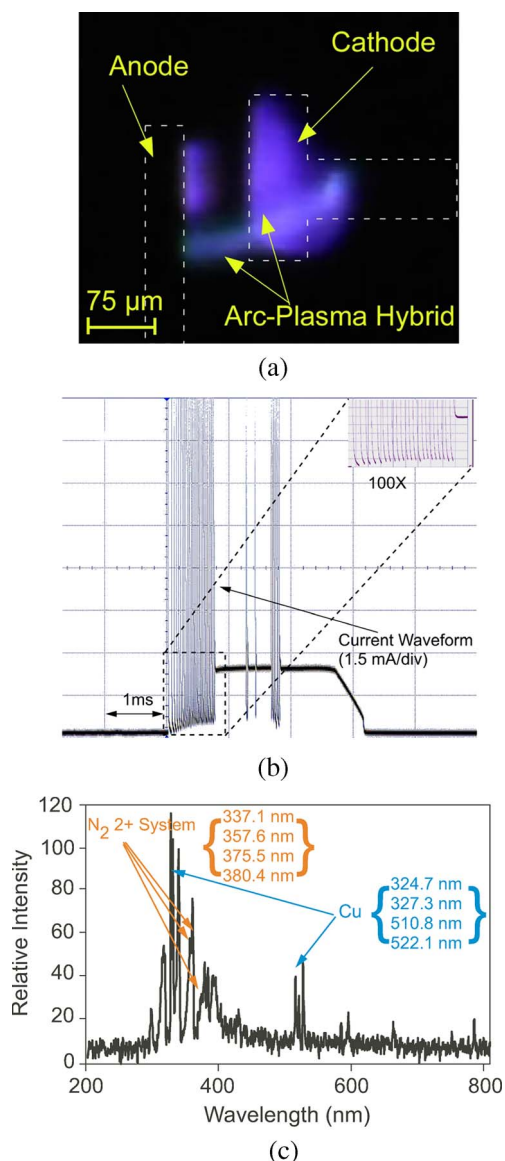


Fig. 5. (a) Example of an arc–glow discharge hybrid, showing both components. (b) The current waveform shows both transient and steady components corresponding to the two types of discharges. (c) The emission spectrum is a mix of both glow and arclike spectra, having emission both in the UV–blue and green regions. Emission lines from both copper (324.7, 327.3, 510.8, and 522.1 nm) and nitrogen (337.1, 357.6, 375.5, and 380.4 nm) can be seen.

which is much weaker. The surge in current is due to the formation of cathode spots (lasting a few microseconds) that are formed on the cathode surface [27]. These discharges are different from pure arc discharges, which occur when smaller resistance ($< 1\text{ k}\Omega$) and/or higher capacitance is used, and are characterized by much higher currents and no steady (glow) component. Fig. 4(c) shows the spectrum for the aforementioned discharge. Strong lines in the green–red region of the spectrum, which were not present in the spectrum of the glow discharge, become apparent now, but many of the lines present in the UV–blue region of the spectrum are absent. The spectrum shows prominent emission from copper (324.7, 327.33, 510.84, 515.8, and 522.07 nm).

With an intermediate current-limiting resistor, the discharge shows both arclike and glowlike components. Fig. 5(a) shows a photograph of a typical discharge. A glow discharge over the

electrodes and an arclike discharge in the gap region, corresponding to the arc/glow portions of the discharge, respectively, can be seen. When seen optically, the discharges are simultaneous, but the waveforms suggest that the arclike discharges might occur as instabilities in the glow discharge. Fig. 5(b) shows the current waveforms for the discharge, with the limiting resistor being set to 33 k Ω . The current waveform shows both a steady (glow) and an erratic (arc) component. Fig. 5(c) shows the spectrum in air when a hybrid discharge was initiated when using a 33-k Ω limiting resistor. This spectrum contains both long and short wavelength lines corresponding to both arclike and glowlike components. The spectrum contains lines from both copper and nitrogen.

Pulsed discharges are not just short-duration dc discharges. They differ from dc discharges in significant ways. In a pulsed discharge, the interval between pulses affects the nature of discharge considerably. DC discharges tend to be arclike, even for resistances as high as 200 k Ω . In pulsed discharges, if the interval between pulses is short (typically 2 s or lower), significant variations are observed from one pulse to the next. For example, there can be a cyclical variation in breakdown voltage, and the discharge alternates between being arclike and glowlike. This is because each pulse is affected by the pulse preceding it in a significant way. This variation may be attributed to electrode and gas heating effects, which persist after the current has been turned off. These tend to lead the glowlike discharge to degenerate into arclike discharges. In arc discharges, electrode degradation occurs at the electrode hot spot, so arcs revert back to glow discharges in the next pulse. Instead of the device settling in a stable equilibrium discharge, a cyclical variation is seen. When the interval between pulses is large (> 5 s), the effect of the previous pulse is not as important, and the discharge tends to be more stable.

B. Microdischarge Devices

The gas discharge microchip [Fig. 1(a)] consists of planar copper microelectrodes fabricated on a glass (Pyrex #7740) substrate. The anode–cathode (A–K) gap spacing is 75 μm . The cathode is designed to have a large area (300 $\mu\text{m} \times 300 \mu\text{m}$), as microdischarges are driven mainly by secondary emission from the cathode. Some designs have a shaped anode to provide a consistent breakdown path for the arc. Devices with a rectangular strip of wire as anode (and same discharge gap) were also fabricated and showed identical results.

In the liquid discharge microchip [Fig. 1(b)], a microdischarge is struck between a metal anode and a porous glass cathode. The porous cathode is wetted by the conductive aqueous sample, which is added through a side port in the chip. The metal impurities in the wet electrode are sputtered into the discharge and undergo atomic transitions (which result in characteristic line spectra) in the plasma glow. The porous cathode allows for controlled uptake of the liquid sample, which eliminates splashing of the liquid, and thus increases device reliability at smaller A–K gaps (the electrode spacing between the metal electrode and the porous cathode is 75 μm). The smaller A–K gaps also enable the use of atmospheric-pressure glow discharges rather than arcs. It is notable that

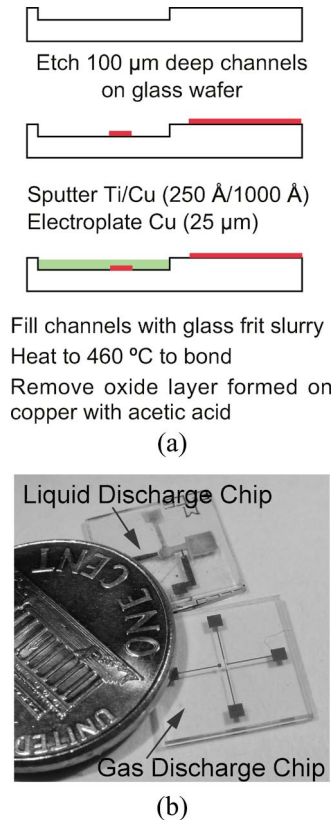


Fig. 6. (a) Process for the fabrication of the liquid microdischarge chip. The fabrication for the gas discharge microchip involves only step 2. (b) Photograph of the liquid and gas microdischarge chips shown against a U.S. penny.

glow microdischarges are driven, to a large extent, by secondary emission from the cathode, so the use of the cathode as a means of sample delivery results in a very sensitive device. While the concept of discharge-based detection of inorganic impurities in water was described in [16], that effort used a liquid microchannel for the cathode rather than a porous cathode. The porous cathode provides the benefit of wicking the aqueous sample for delivery from a side port to the discharge region.

C. Microfabrication Process

Both the GDM and the LDM use electroplated copper electrodes on a glass substrate. For the GDM, a blanket Ti/Cu (50 nm/100 nm) sputtered deposition is used as the base layer. A layer of photoresist (Clariant, AZ9260) is used to define a 50- μm -thick mold for the plating. A layer of copper, 25 μm thick, is then electroplated through the mold to define the electrodes. The photoresist and the base layers are then etched away to leave the electrode structure intact.

The LDM fabrication [Fig. 6(a)] begins with a glass etch to define a 55- μm -deep recess for the porous cathode. A layer of Cr/Au (50 nm/500 nm) is used as the etch mask. Then, the copper electrodes are electroplated, as in a GDM, to form the anode and cathode contact, respectively. Finally, the porous cathode is fabricated by filling channels with glass frit slurry in acetone (0.2 g/mL), followed by sintering in a furnace at 460 $^{\circ}\text{C}$ for 20 min. A layer of oxide is formed over the electroplated copper during sintering. The oxide layer is removed by etching it in acetic acid at 45 $^{\circ}\text{C}$ for 30 min. Fig. 6(b) shows

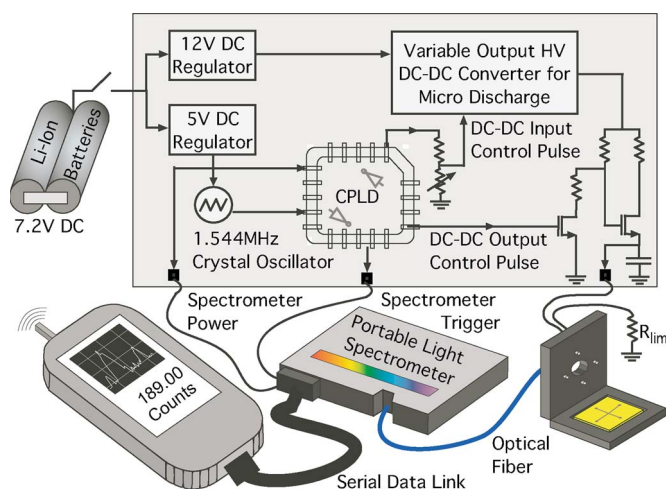


Fig. 7. Schematic of the handheld system. The chip is placed in the chip holder, and the discharge is struck using the control circuit. The spectrometer captures the optical signal and transfers the data to a wireless-enabled PDA on a serial link. (Inset) The controller circuit.

the fabricated GDM and LDM devices against a U.S. penny. The devices have an overall footprint of $1\text{ cm} \times 1\text{ cm}$.

III. SYSTEM DESIGN

The handheld system (Fig. 7) includes a sensor chip holder, a pager-sized spectrometer (USB 2000 from Ocean Optics), a PDA (HP IPAQ HX 2000 Pocket PC), and a battery-operated control circuit and power management unit. The sensor chip holder can accommodate both liquid and gas microdischarge chips, which can be easily swapped in and out. This is implemented by mounting the chips on a PCB and making contact to it by spring-loaded contacts in the customized chip holder unit, which is made from Noryl plastic (G.E. Plastics). The sensor chip holder also has a strategically placed collimating lens (Ocean Optics, UV-74, with a diameter of 5 mm, a focal length of 10 mm, and fused-silica construction for 200–2000-nm wavelength) for coupling the microdischarge emission to an optical fiber (which connects to a spectrometer). This arrangement provides easy optical alignment and maximum light transfer to the optical fiber.

A custom circuit provides the necessary pulses for the discharge and the data acquisition so that the spectroscopic data are captured and transferred to the wireless-enabled handheld computer (PDA) at each discharge event. The control circuit is designed to achieve accurate timing of low- and high-voltage pulses for creating the discharge and synchronizing the optical sampling with controlled delay and duration. The system is powered by two rechargeable 3.6-V Li-ion batteries. These batteries were selected for their long lifetime and ability to provide high current. The unregulated voltage from the battery is sent to two regulators, so that the circuit supply voltage remains constant for battery voltages ranging from 6.5 to 8.4 V. A 5-V linear regulator (LP 8345 from National Semiconductors) powers the complex programmable logic device (CPLD) and the spectrometer. A linear regulator was chosen (even though it is not power efficient) because the spectrometer requires a low-noise power supply for accurate data acquisition. A second

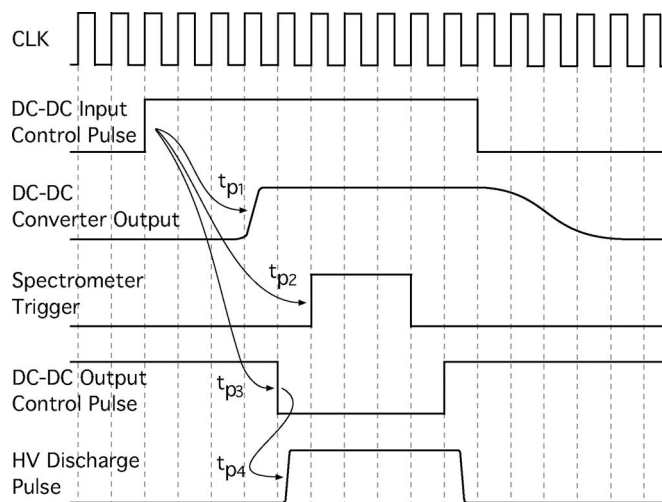


Fig. 8. Operating cycle of the system. The discharge pulse is controlled control signals to the input and output of the dc–dc converter. The timing is accurate to $50\ \mu\text{s}$.

dc–dc converter (MAX1771 from Maxim) generates a 12-V output, with up to 500-mA current, which is provided to yet another dc–dc converter (described later) for generating the higher voltages required for initiating discharge. The 12-V output can be changed by adjusting a potentiometer. Because the high-voltage section requires significant current, and power supply noise is not significant, this approach provides overall power efficiency.

A 1.544-MHz crystal oscillator provides the reference clock for the digital circuit. The actual clock is stepped down in frequency from the reference clock by using ripple counters. This is done to allow software control of the operating frequency and, hence, the minimum and maximum pulse timings.

Dedicated hardware control of the discharge and sampling trigger pulses is necessary because accurate triggering requires low jitter in the pulses. Programmability is essential as the timing requirements can vary depending upon the application. The use of a CPLD (Atmel ATF1508AS) for digital logic provides both accuracy and reconfigurability. The system is designed to have three output pulses, which can start at and last for separately programmed clock cycles. While independent, they use the same clock for synchronization. The start time of each pulse is hard programmed into the CPLD, but the pulse durations can be modified using a series of DIP switches outside the CPLD. The CPLD is operated at a frequency of 24.125 kHz, which corresponds to a pulse accuracy of $45.451\ \mu\text{s}$.

Fig. 8 shows the overall timing scheme for the system. In order to prevent the inadvertent triggering of a pulse from power-up conditions, an RC combination is used to provide a 5-ms ramp to a reset input in the CPLD. The outputs from the CPLD are used to trigger the high-voltage section of the circuitry and the spectrometer. The high-voltage dc–dc converter (HVP2P from Pico Electronics), which powers the microdischarge, generates 250–2000 V from the 12-V input previously described. The output voltage is controlled by a proportional input, which has a linearity error of $< 1\%$. For example, 2.5 V at this input corresponds to an output voltage of 1000 V, whereas a 5-V input corresponds to an output voltage of

2000 V. The output voltage is designed to fall to 0 V when the programmable input falls below 0.25 V. To trigger the output pulse, the 5-V trigger signal from the CPLD is sent through a voltage divider and then into the programmable input. In this design, the input would be at 0 V for a period of time, then the trigger pulse would move this input to a designed voltage for the desired output voltage, and then back to 0 V.

The output of the dc–dc converter can be optionally controlled by a shunt–series switch. Because the dc–dc converter has finite rise and fall times, applications in which faster transitions are required would benefit from this approach. The signal from the high-voltage converter is fed into a high-speed MOSFET-controlled switching circuit that uses two transistors, as shown in Fig. 7. These MOSFETs (STP3NB100 from STMicroelectronics) allowed for a maximum V_{DS} of 1000 V, with a V_{GS} of only 5 V, and have an “on” resistance of $< 6 \Omega$. A 0-V output control pulse on the gate of the shunt transistor permits the discharge electrode to receive power, whereas a 5-V gate bias on the same line activates the shunt to ground. The timing for this is shown in Fig. 8.

This system permitted the control of the spectrometer and high-voltage outputs individually to an accuracy of $< 50 \mu\text{s}$, with pulse durations from $50 \mu\text{s}$ to just under 1 s. It is notable that the accuracy and the maximum pulse periods are both determined by the clock speed, and the use of a software-controlled clock allows one to trade off one for the other. An accuracy of 10 ns in timing is possible just by programming the CPLD accordingly. However, in such a case, the maximum pulse duration can only be 0.5 ms due to the interdependent nature of these two variables.

The handheld system and its components are shown in Fig. 9. The overall dimensions of the system are approximately $19 \times 13 \times 5 \text{ cm}^3$, but there is substantial room for further miniaturization. The handheld spectrometer, with a range of 200–850 nm in wavelength, is approximately $9 \times 6 \times 3 \text{ cm}^3$, and the chip holder is $4 \times 4 \times 2 \text{ cm}^3$.

IV. MEASUREMENT RESULTS

The electrical characterization of the discharge was performed by varying the applied voltage and limiting resistor. The I – V curve for the glow component (Fig. 10) is obtained by measuring the current through the discharge with different biases and limiting-resistor values. No breakdown takes place for voltages less than 460 V. Larger voltages show increasing current, with a differential resistance of 80 k Ω . The external circuit is represented by the load line on the I – V curve. The system settles to a point at the intersection of the load line and the device I – V curve, so a particular state can be achieved by controlling either the overvoltage or the resistor. This I – V curve is valid only for resistance values between 1 k Ω and 1 M Ω . Below 1-k Ω resistance, the discharge is dominated completely by the arc component.

The arc component of the discharge is not a strong function of applied voltage. Arcs are generally driven by current rather than voltage, and these discharges are no exception. The arclike discharge is powered from the energy stored in the capacitor. Even if no capacitor is used, the parasitic capacitance of the

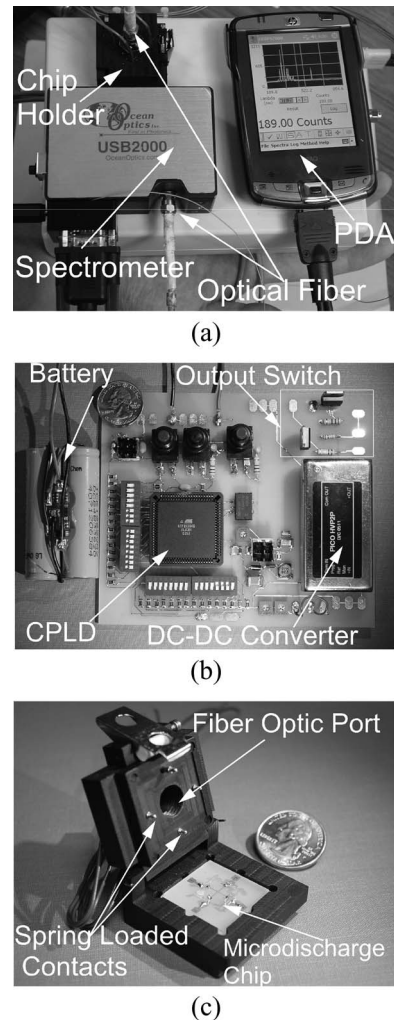


Fig. 9. (a) Photograph of the handheld system showing the controller, the chip holder, and the PDA. (b) Photograph of the controller circuit. (c) Photograph of the chip holder shown against a U.S. quarter. Contact to the terminals is made mechanically by a spring-loaded gold-plated pin. A lens is placed in the middle, which is aligned with the active area.

device ($\sim 2 \text{ pF}$) supplies the energy (the initiation of breakdown is erratic when not using parasitics, so a small capacitor is used in the operation). The capacitor oscillates between the glow discharge breakdown voltage and the arc breakdown voltage. The power delivered by the capacitor is given by $P_c = CV_{\text{bkdn}}\Delta V/\tau$, where τ is the time constant, V_{bkdn} is the breakdown voltage, and ΔV is the amplitude of the voltage oscillations. The reason for the oscillation is not known but is probably due to the expansion of the cathode spots [27]. It is a weak function of power, as oscillations occur even when using large resistors. The oscillation is a strong function of pressure, as discharges at lower pressures ($\sim 450 \text{ torr}$) are glow discharges.

The time constant of the discharge is related to the time constant of the discharge resistor. Fig. 10(b) shows the plot of the measured time constants for the arclike discharge for various limiting resistors. The time constants were obtained by fitting the current waveform to a decaying exponential. It is seen that the time constant is linearly related to the limiting resistor.

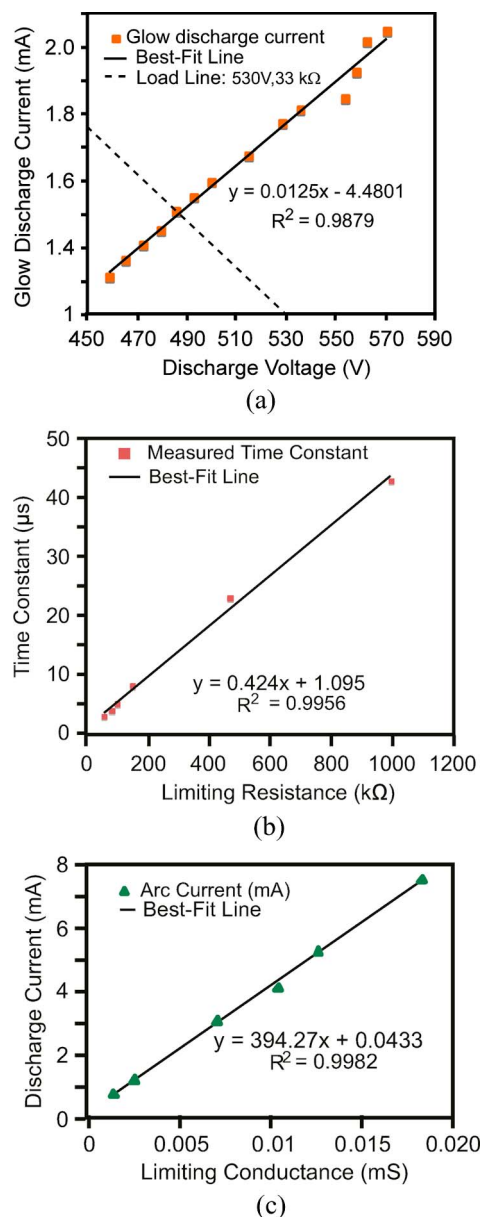


Fig. 10. (a) I - V curve for the glow discharge component of the discharge. (b) Time constant of the arclike component as a function of limiting resistance. (c) Discharge current for the arclike component as a function of limiting resistance.

The effect of inductance is evaluated by measuring the time constant for a variable inductor placed between the cathode and limiting resistor. No significant change is observed in the time constant when the inductance is varied from zero to $2 \mu\text{H}$. The time constant is not related to the inductance of the arc in this case, contrary to traditional arc models where arc inductance plays a major role in the duration of the discharge [29]. The addition of a small inductor leads to a ringing in the arc waveform, with a high-frequency ac component being superposed on the decaying exponential. However, this does not have an effect on the powering of the arc.

The time constant is related to the capacitance in a complex way. On increasing the capacitance from 15 to 25 pF, the time constant changed from 6.53 to 8.61 μs . However, increasing the capacitance to 50 pF led to discharge instability, and the

discharge was no longer an arc-glow hybrid but an intermittent arc discharge. The hybrid discharge thus operates only in a narrow range of capacitance values, and higher values of capacitance are likely to lead to nonlinear effects which result in a runaway process.

The arc-like component of the current in the discharge depends upon the value of the limiting resistor. Fig. 10(c) shows the plot of the arc current versus the conductance of the limiting resistor. The fit shows a linear relationship between the arc current and conductance of the limiting resistor. It is thus seen that the limiting resistor can be used to control the current of the arclike discharge. It is noteworthy that the arc current does not depend upon the overvoltage. For the case of using a 1-M Ω resistor, the increase in applied voltage from 630 to 700 V did not lead to a change in arc current. This result is important because, as shown earlier, the glow discharge component strongly depends upon the overvoltage. Thus, by using a proper combination of limiting resistor, the arc and glow components of the hybrid discharge can be controlled.

While the power of individual pulses in the arclike discharge can be controlled by using circuit elements, the number of arclike pulses is difficult to control. The number of pulses is lower for higher resistances, but there is still significant variation between pulses. This is probably because the effect itself is as a result of some instability in the discharge process. It is clearly seen that the discharge is predominantly glowlike at lower pressures (~ 450 torr), which suggests that it is probably related to heating by electron-neutral collisions. The electrode material also has a significant impact on the nature of the discharge. When using iridium instead of copper, a predominantly arclike discharge was observed.

To evaluate the hybrid micro arc-glow device as a vapor sensor, the devices were placed in a chamber into which acetone vapor samples were introduced. Air was used as a carrier gas, and the pressure inside the chamber was maintained at 810 torr. A vacuum pump was used to evacuate the chamber from impurities before the experiment but was not used during the experiment. A commercial vapor sensor (MiniRAE 2000) was used as a benchmark.

The device was operated in hybrid mode, with the limiting resistor being set to 22 k Ω . A hybrid discharge was chosen, as it had the strongest emission in the wavelength range of interest (350–450 nm). One-shot detection was performed, with pulse duration of 45 ms.

Fig. 11(a) shows a portion of a typical microdischarge spectrum (300–400 nm) taken in 17-ppm ambient of acetone. In the absence of preconcentration of sample vapors, this is a significant challenge for a microsensor, particularly when using portable optics. The spectrum shows a line at 388.6 nm that corresponds to CN fragments produced from acetone in the air microdischarge [30]. This line is absent from the control spectra taken in air [Fig. 11(b)], and at high concentrations, it dwarfs all the other lines. Note that the spectra are normalized to the strongest line. In the spectrum for 4000-ppm acetone, as shown in Fig. 11(c), the nitrogen lines seem diminished, not because the nitrogen emission is diminished but because the carbon line is very intense due to the high vapor concentration.

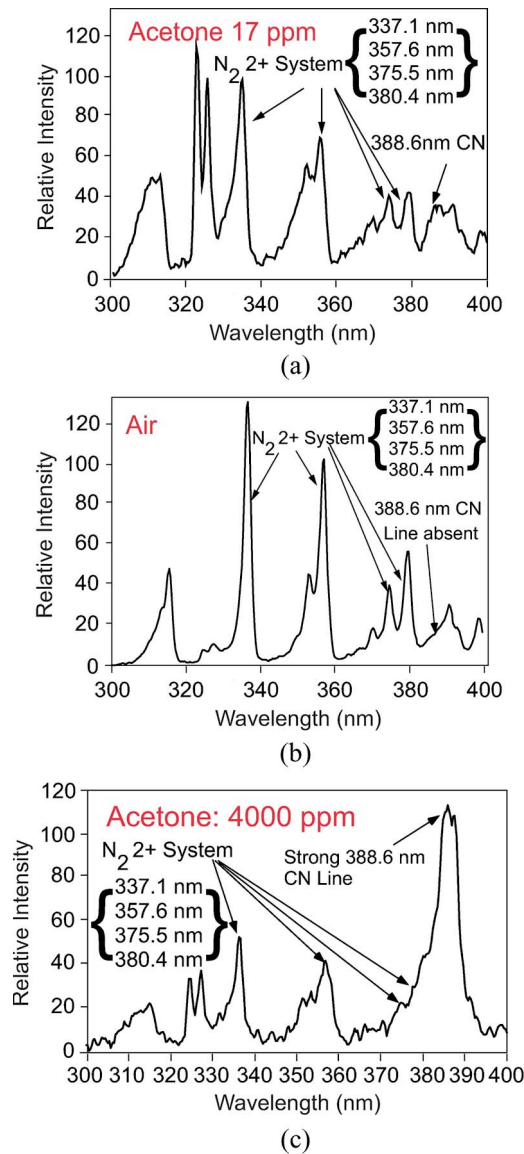


Fig. 11. Spectra from the gas discharge microchip (without preconcentration). (a) In 17-ppm acetone showing the presence of 388.6-nm emission from carbon containing fragments. (b) Control experiment in air. The 388.6-nm line is absent. (c) The relative intensity of 388.6 nm is much more with higher acetone concentration.

A response curve for acetone [Fig. 12(a)] can be obtained by measuring the 388.6-nm line intensity for different concentrations of acetone. The background signal on which the line is superposed is accounted for by subtracting the average of line intensities at two inflection points (390.3 and 387.28 nm) from the line intensity at 388.6 nm. This is normalized to the 391.4-nm nitrogen line to compensate for the optical power of the discharge [2]. The calculation, shown graphically in Fig. 12(b), is represented by

$$\text{Line_Strength (388.6 nm)} = \frac{I(388.6) - \left(\frac{I(390.3) + I(387.28)}{2} \right)}{I(391.4)} \quad (2)$$

Because the lines are close together, variations in the electron energy distribution function between different discharges are

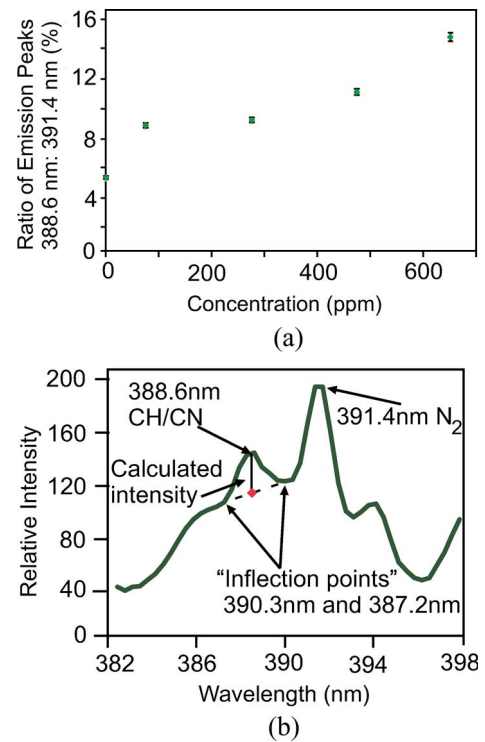


Fig. 12. (a) Response curve showing variation in the normalized CN (388.6-nm) line intensity as a function of acetone concentration. The line strength is normalized to 391.47-nm nitrogen line to account for variation in optical intensity of the discharge. The data at 0 ppm represents the control signal in air. (b) Calculation of the line intensity. The 388.6-nm line is superposed on a background signal. The background compensated for by subtracting the average of line intensities at two inflection points (390.3 and 387.28 nm) from the line intensity at 388.6 nm.

not likely to significantly affect their intensity ratio. Additionally, the relative line strength is not expected to increase linearly with acetone concentration because cross sections for excitation by electron impact are likely to be different for the CN and nitrogen molecules. At pressures approaching atmospheric pressure, stepwise excitation and ionization processes become a significant source of excitation (these occur by multiple collisions with low-energy electrons instead of a single collision with a high-energy electron). Furthermore, the formation of the fragment species is dependent on the energy of the discharge, so the response curve is not expected to be linear. It may be noted that circuit configuration in all the experiments is the same, and the normalization only corrects for a small pulse-to-pulse variation in power.

For evaluating the LDM, the standard that was used contained 2-ppm Cr in an aqueous solution that also had 5% HNO₃. This was a mixture of 2 μ L of 10000-ppm plasma standard Cr in 5% HNO₃ (Specpure) and 10 mL of 5% HNO₃. In a typical experiment, a 1- μ L sample was loaded through the side port, which was wicked to the discharge site through the porous electrode material. The sample was loaded only once to avoid inadvertent preconcentration. Fig. 13 shows a typical spectrum, having emission from the 427.6-nm Cr line [31] which is missing from the control sample of 5% HNO₃. The spectra also showed a strong 325-nm line emission (not shown in the figure) from the copper in the anode material and

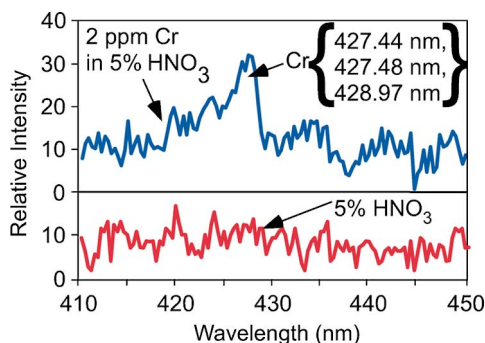


Fig. 13. Spectra from the liquid spectroscopy microchip (obtained without preconcentration). An emission line at 427.5 nm due to (top) chromium is clearly seen. (Bottom) The control sample shows no emission at that wavelength.

copper oxide additive in glass frit (this has no impact on the sensor as long as Cu is not the target chemical of interest).

The sensitivity of the overall measurement can be further increased by using preconcentration. In such a mode, the sample is repeatedly loaded and allowed to dry. The metal salt accumulates at the cathode and hence gives a stronger signal. Another consequence of preconcentration is that the pH gradually increases due to acid accumulation. It is well known that the microdischarge device shows better performance at lower pH [20], so this helps getting better sensitivity without using a highly acidic sample.

The measurements suggest that the sensitivity of the LDM is slightly higher compared to devices employing a liquid cathode [19], which could detect about 10 ppm of Cr. The use of a porous cathode is also attractive because it eliminates the motion of the liquid and the potential for spillover at the cathode site (which improves reliability) and improves the consistency of data across pulses by a much better controlled injection of the liquid sample into the discharge glow.

V. CONCLUSION

Pulsed microscale discharges at atmospheric pressure can occur as glow discharges, as arc discharges, or as a combination of the two in the form of arc-glow hybrids. The presence of a stable intermediate between arcs and glows is a feature of microdischarges. The characteristics of the discharge can be easily tuned, to enhance spectral output in a given region of the spectrum, by a simple control circuit.

Sensors based on microdischarge spectroscopy are promising because they can detect a wide range of chemicals almost instantaneously. This paper demonstrates the possibility of a handheld microdischarge-based chemical analysis system for sensing in gaseous and liquid environments. The system employs swappable gas and liquid microdischarge chips and a chip holder that interfaces to both, providing a low impedance contact and automatic optical alignment to the discharge. The microdischarges operate at atmosphere in air ambient, eliminating the need for a pump or special gases for the analysis. The gas discharge microchip can detect 17 ppm of acetone vapor in air ambient. The liquid discharge microchip demonstrates the first use of a wet porous cathode. The porous cathode introduces

controlled amount of sample by wicking in liquid through the pores while still providing low impedance to the cathode contact. This eliminates splashing of the liquid and increases device reliability and sensitivity over discharges, which employ a liquid electrode. Using this chip and the handheld system, the detection of 2 ppm of Cr was demonstrated.

ACKNOWLEDGMENT

The authors would like to thank W. Zhu for the help with the fabrication of the devices and R. Fung for the help with machining of the chip holder. We would also like to thank Prof. J. Foster for the valuable discussions regarding the physics of discharges.

REFERENCES

- [1] D. S. Wilson, S. Hoyt, J. Janata, K. Booksh, and L. Obando, "Chemical sensors for portable, handheld field instruments," *IEEE Sensors J.*, vol. 1, no. 4, pp. 256–274, Dec. 2001.
- [2] J. Janata, "Electrochemical microsensors," *Proc. IEEE*, vol. 91, no. 6, pp. 864–869, Jun. 2003.
- [3] J. W. Gardner and P. N. Bartlett, *Electronic Noses: Principles and Applications*. Oxford, U.K.: Oxford Univ. Press, 1999.
- [4] C.-J. Lu, W. H. Steinecker, W.-C. Tian, M. C. Oborny, J. Nichols, M. Agah, J. A. Potkay, H. K. Chan, J. A. Driscoll, R. D. Sacks, K. D. Wise, S. W. Pang, and E. T. Zellers, "First-generation hybrid MEMS gas chromatograph," *Lab Chip*, vol. 5, no. 10, pp. 1123–1131, Aug. 2005.
- [5] G. Frye-Mason, R. Kottenstette, C. Mowry, C. Morgan, R. Manginell, P. Lewis, C. Matzke, G. Dulleck, L. Anderson, and D. Adkins, "Handheld miniature chemical analysis system (μ ChemLab) for detection of trace concentrations of gas phase analytes," in *Proc. Micro Total Anal. Syst. Workshop*, M. Ramsey, A. van den Berg, Eds., May 2001, pp. 658–660.
- [6] C. B. Freidhoff, R. M. Young, S. Sriram, T. T. Braggins, T. W. O'Keefe, J. D. Adam, H. C. Nathanson, R. R. A. Syms, T. J. Tate, M. M. Ahmad, S. Taylor, and J. Tunstall, "Chemical sensing using nonoptical microelectromechanical systems," *J. Vac. Sci. Technol. A, Vac. Surf. Films*, vol. 17, no. 4, pp. 2300–2307, Jul./Aug. 1999.
- [7] S. Taylor, B. Srigengan, J. R. Gibson, D. Tindall, R. Syms, T. J. Tate, and M. M. Ahmad, "A miniature mass spectrometer for chemical and biological sensing," *Proc. SPIE*, vol. 4036, pp. 187–193, 2000.
- [8] R. A. Miller, E. G. Nazarov, G. A. Eiceman, and A. T. King, "A MEMS radio-frequency ion mobility spectrometer for chemical vapor detection," *Sens. Actuators A, Phys.*, vol. 91, no. 3, pp. 301–312, Jul. 2001.
- [9] G. E. Spangler and R. A. Miller, "Application of mobility theory to the interpretation of data generated by linear and RF excited ion mobility spectrometers," *Int. J. Mass Spectrom.*, vol. 214, no. 1, pp. 95–104, Feb. 2002.
- [10] E. H. Evans, J. A. Day, W. J. Price, C. M. M. Smith, and K. Sutton, "Atomic spectrometry update. Advances in atomic emission, absorption and fluorescence spectrometry, and related techniques," *J. Anal. At. Spectrom.*, vol. 18, no. 7, pp. 672–711, 2003.
- [11] V. Karanassios, "Microplasmas for chemical analysis: Analytical tools or research toys?" *Spectrochim. Acta B, At. Spectrosc.*, vol. 59, no. 7, pp. 909–928, Jul. 2004.
- [12] J. A. C. Broekaert, "The development of microplasmas for spectrochemical analysis," *Anal. Bioanal. Chem.*, vol. 374, no. 2, pp. 182–187, Sep. 2002.
- [13] J. Hopwood, "A microfabricated inductively coupled plasma generator," *J. Microelectromech. Syst.*, vol. 9, no. 3, pp. 309–313, Sep. 2000.
- [14] F. Iza and J. Hopwood, "Low-power microwave plasma source based on a microstrip split-ring resonator," *IEEE Trans. Plasma Sci.*, vol. 31, no. 4, pp. 782–787, Aug. 2003.
- [15] S. J. Park, J. Chen, C. Liu, and J. G. Eden, "Silicon microdischarge devices having inverted pyramidal cathodes: Fabrication and performance of arrays," *Appl. Phys. Lett.*, vol. 78, no. 4, pp. 419–421, Jan. 2001.
- [16] J. C. T. Eijkel, H. Stoeri, and A. Manz, "A DC microplasma on a chip employed as an optical emission detector for gas chromatography," *Anal. Chem.*, vol. 72, no. 11, pp. 2547–2552, Jun. 2000.

- [17] T. Cserfalvi, P. Mezei, and P. Apai, "Emission studies on a glow discharge in atmospheric pressure air using water as a cathode," *J. Phys. D, Appl. Phys.*, vol. 26, no. 12, pp. 2184–2188, Dec. 1993.
- [18] B. Mitra and Y. B. Gianchandani, "The micromachined FlashFET: A low-power, three-terminal device for high speed detection of vapors at atmospheric pressure," in *Proc. IEEE Int. Conf. MEMS*, Miami, FL, 2005, pp. 794–797.
- [19] L. Que, C. Wilson, and Y. B. Gianchandani, "Microfluidic electrodischarge devices with integrated dispersion optics for spectral analysis of water impurities," *J. Microelectromech. Syst.*, vol. 14, no. 2, pp. 185–191, Apr. 2005.
- [20] C. G. Wilson and Y. B. Gianchandani, "Spectral detection of water contaminants using an on-chip microglow discharge," *IEEE Trans. Electron Devices*, vol. 49, no. 12, pp. 2317–2322, Dec. 2002.
- [21] C. G. Wilson, Y. B. Gianchandani, R. R. Arslanbekov, V. Kolobov, and A. E. Wendt, "Profiling and modeling of DC nitrogen microplasmas," *J. Appl. Phys.*, vol. 94, no. 5, pp. 2845–2851, Sep. 2003.
- [22] M. J. Kushner, "Modelling of microdischarge devices: Plasmas and gas dynamics," *J. Phys. D, Appl. Phys.*, vol. 38, no. 11, pp. 1633–1643, Jun. 2005.
- [23] B. Mitra and Y. B. Gianchandani, "Microdischarge–microplasma hybrids for detection of vapors at atmospheric pressure," in *Proc. IEEE Conf. Sensors*, Irvine, CA, Nov. 2005, pp. 326–329.
- [24] B. Mitra, B. Levey, T.-C. Fung, and Y. B. Gianchandani, "A handheld microdischarge spectroscopy system for high-speed chemical analysis of gaseous and liquid samples," in *Proc. IEEE/ASME Int. Conf. MEMS*, Istanbul, Turkey, Jan. 2006, pp. 554–557.
- [25] Y. P. Raizer, *Gas Discharge Physics*. Berlin, Germany: Springer-Verlag, 1997.
- [26] P. Gill and C. E. Webb, "Electron energy distributions in the negative glow and their relevance to hollow cathode lasers," *J. Phys. D, Appl. Phys.*, vol. 10, no. 3, pp. 299–311, Feb. 1977.
- [27] M. M. Kekez, M. R. Barrault, and J. D. Craggs, "Spark channel formation," *J. Phys. D, Appl. Phys.*, vol. 3, no. 12, pp. 1886–1896, Dec. 1972.
- [28] A. Anders and S. Anders, "On modes of arc cathode operation," *IEEE Trans. Plasma Sci.*, vol. 19, no. 1, pp. 20–24, Feb. 1991.
- [29] R. T. Robiscoe, A. Kadish, and W. B. Maier, II, "A lumped circuit model for transient arc discharges," *J. Appl. Phys.*, vol. 64, no. 9, pp. 4355–4363, Nov. 1988.
- [30] R. W. B. Pearse and A. G. Gaydon, *The Identification of Molecular Spectra*, 3rd ed. London, U.K.: Chapman & Hall, 1963, pp. 28–29.
- [31] W. F. Meggers, C. H. Corliss, and B. F. Scribner, *Tables of Spectral Line Intensities, Part 1*. Washington, DC: GPO, 1975. NBS Monograph 145.



Bhaskar Mitra received the B.Tech. and M.Tech. degrees in electrical engineering from the Indian Institute of Technology, Bombay, India, in 2002, and the Ph.D. degree from the University of Michigan, Ann Arbor, in 2008.

He is currently with the Department of Electrical Engineering and Computer Science, University of Michigan, Ann Arbor. His Ph.D. research focused on the study of microdischarges and their application to chemical sensing in liquid and gas ambient. His areas of interests include the study of physical phenomena

at micrometer scales and the design of microsystems for chemical and biological sensing.

Brandon Levey received the B.S. and M.S. degrees in electrical engineering from the University of Michigan, Ann Arbor, in 2004 and 2006, respectively.

Since then, he has been with Sandia National Laboratories, Albuquerque, NM.



Yogesh B. Gianchandani received the B.S., M.S., Ph.D. degrees in electrical engineering, with a focus on microelectronics and MEMS.

He is currently a Professor with the University of Michigan, Ann Arbor, with a primary appointment in the Department of Electrical Engineering and Computer Science and a courtesy appointment in the Department of Mechanical Engineering. He is temporarily with the National Science Foundation, Arlington, VA, as the Program Director within the Electrical, Communication, and Cyber Systems Division.

He was previously with the University of Wisconsin, Madison. He also held industry positions, working in the area of integrated circuit design. His research interests include all aspects of design, fabrication, and packaging of micromachined sensors and actuators and their interface circuits. He is the author of approximately 200 papers in journals and conference proceedings and is the holder of about 30 issued or pending U.S. patents. He was a Chief Coeditor of *Comprehensive Microsystems: Fundamentals, Technology, and Applications* (Elsevier, 2007). He serves on the editorial boards of several journals.

Dr. Gianchandani was a General Cochair of the IEEE/ASME International Conference on Micro Electro Mechanical Systems in 2002.